*Proceedings of ITC18,2008*

# Configuration effect on energetic particle and thermal energy confinement in NBI plasmas of Heliotron J

S. Kobayashi[1)], T. Mizuuchi[1)], K. Nagasaki[1)], H. Okada[1)], K. Kondo[2)], S. Yamamoto[1)], S. Murakami[3)], D. Katayama[2)], Y. Suzuki[4)], T. Minami[4)], K. Nagaoka[4)], Y. Takeiri[4)], K. Murai[2)], Y. Nakamura[2)], M. Yokoyama[4)], S. Konoshima[1)], K. Hanatani[1)], G. Motojima[4)], K. Hosaka[2)], K. Toushi[1)], F. Sano[1)]

*1) Institute of Advanced Energy, Kyoto University, Gokasho, Uji 611-0011, Japan*

*2) Graduate School of Energy Science, Kyoto University, Gokasho, Uji 611-0011, Japan*

*3) Graduate School of Engineering, Kyoto University, Kyoto 606-8501, Japan*

*4) National Institute for Fusion Science, Toki, Gifu, 509-5292, Japan*

The configuration effect on the energetic ion and the global energy confinement has been investigated in the NBI plasmas of Heliotron J with regard to the effect of the bumpy magnetic field (bumpiness) being the key factor of the drift optimization in the helical-axis heliotron configuration. The configuration scan experiments have been carried out by changing the bumpy magnetic field ($\varepsilon_b$) with keeping plasma volume, plasma axis position and edge rotational transform almost constant. It has been found that the 1/e decay time of high energy CX flux after the NB turned-off has increased with bumpiness. The co-going ion flux of fast ions induced by energetic-ion-driven MHD modes has been observed by installing the hybrid directional Langmuir probe system. The preferable energy confinement time to the international stellarator scaling law ISS95 has been obtained in the high and medium-$\varepsilon_b$ configurations. The improvement in the electron temperature mainly contributes to the enhancement of the plasma performance in the high- and medium-$\varepsilon_b$ configurations The control of bumpiness is effective not only in the energetic particle transport but also in the global energy confinement in NBI plasmas of Heliotron J.

Keywords: Helical-axis heliotron configuration, Heliotron J device, neutral beam heating, drift optimization, bumpiness magnetic field component, energetic particle confinement and energy confinement.

## 1. Introduction

For the optimization of helical/stellarator magnetic configurations toward the fusion reactor, it is important subject to reduce the ripple loss of helically trapped particle and to control the neoclassical transport since the magnetic field has the three-dimensional structure. The configuration optimization in terms of “drift optimization” has been achieved by aligning the drift orbit surface to the magnetic flux one. In the planner axis heliotron configurations such as LHD, Heliotron E and CHS [1-3], the drift orbit surface has been optimized when the magnetic axis was shifted inwardly and the reduction in neoclassical transport coefficient in the $1/\nu$ regime has been found [4]. From the viewpoint of the Boozer coordinate system, the side-band of the helical magnetic field is adjusted in the inwardly-shifted configuration, which plays a key role to reduce the loss of trapped particles. An improvement in the energetic particle confinement has been obtained experimentally in the inward-shifted configuration. In such a case, the enhancement factor of the experimental energy confinement time to the international stellarator scaling (ISS) law has also become better than that of the outward-shifted configurations [5,6]. This suggests that the drift optimization is a candidate to mitigate the anomalous transport.

A helical-axis heliotron device Heliotron J [7,8] is designed based on the omnigeneous optimization scenario [9,10]. In the helical-axis heliotron configuration, the theoretical analysis has predicted that the control of the toroidal mirror ratio, bumpiness, in the Boozer coordinate system has been important for the drift optimization. The neoclassical diffusion coefficient and the loss rate of the energetic particles have had a dependence on bumpiness. Therefore it is important to investigate experimentally the bumpiness effect both on the energetic particle transport and bulk plasma confinement.

In this paper, we describe the configuration effect on the energetic and energy confinement in the NBI plasmas of Heliotron J, focusing on the effects of the bumpy magnetic field. The experimental setup and the characteristics of the configurations used in the bumpiness scan experiments are explained in section 2. The energetic particle transport in the NBI plasmas is shown in section 3. The dependence of the energetic ion transport on bumpiness magnetic field is investigated

*author's e-mail:kobayashi@iae.kyoto-u.ac.jp*

experimentally with charge exchange neutral particle analyzer (CX-NPA). The experimental result of the energetic-ion-driven MHD activities is shown by installation of the hybrid directional Langmuir probe system. The bumpiness effect on the global energy confinement is described in section 4. Summary is given in section 5.

## 2. Experimental Setup

### 2.1. Heliotron J Device

Heliotron J is the medium sized ($R_0/a_p$ = 1.2m/0.17m) helical-axis heliotron device with an $L/M$ = 1/4 helical winding coil, where $L$ and $M$ are the pole number of the helical coil and helical pitch, respectively. Figure 1 shows the bird's-eye view of Heliotron J including the coils and the heating systems. To achieve a flexible configuration control in Heliotron J, five sets of coils are installed, i.e. helical and main vertical (H+V), toroidal A and B (TA and TB) and inner and auxiliary vertical (IV and AV) coils. The TA coils are located at so-called "corner" section where tokamak like magnetic field is formed. On the contrary, the magnetic field in the "straight" section in which the TB coils are set has a local quasi-omnigeneous magnetic field. As shown in Fig. 1, two tangential beamlines of the hydrogen neutral beam injection (NBI) system have been installed in Heliotron J (BL1 and BL2). Each beamline has two bucket-type ion sources and the maximum beam power and acceleration voltage of 0.7 MW and 30 keV, respectively. The mean pitch angle of the beam ions is about 155 (25) degree in the co- (counter-) injection case of the standard configuration of Heliotron J. The numerical analysis of the NBI absorption power is described in section 4. An E//B type CX-NPA system can measure the hydrogen and deuterium charge-exchange neutral fluxes separately. This system also has a capability to scan both poloidal ($\theta_{NPA}$) and toroidal ($\phi_{NPA}$) angles with the ranges of $-3^o < \theta_{NPA} < +10^o$ and $-10^o < \phi_{NPA} < +18^o$. The initial

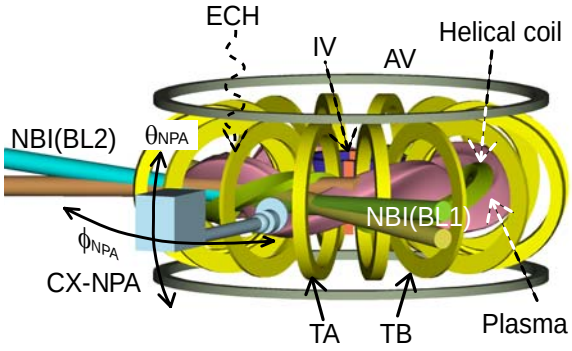


Fig. 1 Schematic view of Heliotron J including coil, heating and diagnostic systems.

plasma is produced by 2nd harmonic 70 GHz ECH with a maximum injection power of 0.4 MW. The deuterium gas was used for working gas to obtain the energy spectra for bulk ($D^+$) and beam ($H^+$) ions separately.

### 2.2. Configuration Characteristics in Bumpiness Scan Experiment

In this study, we selected three bumpiness $\varepsilon_b$ (= $B_{04}/B_{00}$) configurations of high ($\varepsilon_b$ = 0.15), medium (0.06) and low (0.02) at $r/a$ = 2/3 by changing the current ratio of TA and TB coils with keeping the edge rotational transform ($\iota(a)/2\pi$ = 0.56), plasma volume ($V_p$ = 0.7 $m^3$), and magnetic axis position ($R_{ax}$ = 1.2 m) almost constant. Figures 2(a)-(c) show the radial profiles of the magnetic well, bumpiness, helicity $\varepsilon_t$ (= $B_{14}/B_{00}$) and toroidicity $\varepsilon_t$ (= $B_{10}/B_{00}$), where $B_{mn}$ is the Fourier component of the field strength with m/n mode numbers in the Boozer coordinate system. The standard configuration of Heliotron J corresponds to medium-$\varepsilon_b$ configuration. In the low-$\varepsilon_b$ configuration the bumpiness can change its sign in the core region. As shown in Figs. 2(a)-(c), other main Fourier

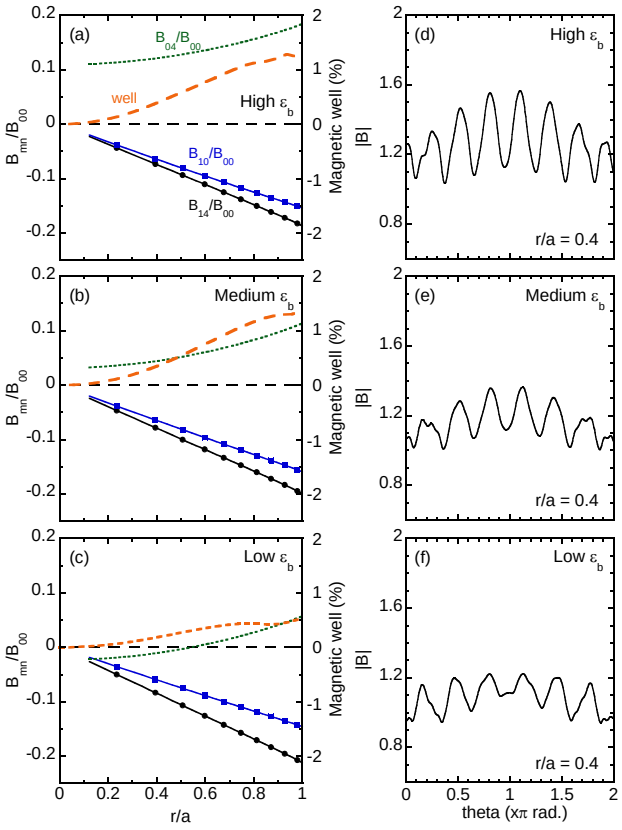


Fig. 2. (a)-(c) Radial profile of magnetic well, helicity, toroidicity and bumpiness in Boozer coordinate systems and (d)-(f) field strength along the field line in the high-, medium and low-$\varepsilon_b$ configurations.

components, i.e. helicity and toroidicity, are almost unchanged to clarify the bumpiness effect on the energy confinement. The magnetic well in the entire plasma region is formed in the three $\varepsilon_b$ configurations. Figures 2(d)-(f) illustrate the magnetic field strength at $r/a$ = 0.4 along a field line in the Boozer coordinate system. In the case of high-$\varepsilon_b$, the ripple amplitude is higher than the others and the minimum values of field strength at the bottoms of the ripple are relatively flat. In contrast, in the configuration with low-$\varepsilon_b$, the strength of the ripple bottoms varies along the field line. From the viewpoint of the Boozer coordinate system, it has been found that the difference between $\boldsymbol{B}$ and $\nabla\boldsymbol{B}$ becomes small as increasing bumpiness [11], which expects the reduction in the gap between drift and flux surfaces in the high-$\varepsilon_b$ configuration.

## 3. Energetic Ion Transport

### 3. 1. Dependence on Bumpiness

The decay of the CX flux just after NB turned-off investigated because this provides information regarding the slowing down and the confinement time of the beam ions [11]. Figure 3(a) shows the time evolution of the CX flux ($E$ = 18 keV) after the NB turned-off for high, medium and low $\varepsilon_b$ cases. The base plasma was sustained by 70 GHz ECH at the line-averaged electron density ($\bar{n}_e$) of $0.8\times10^{19}$ m$^{-3}$. The NPA toroidal angle was set to be $\phi_{NPA}$ = +12 $^o$ to measure the CX flux having more similar pitch angle to the tangentially injected beam ions. The gap between the pitch angle of beam ion and observation one is around 25 degree, since the pitch angle of the detected particle at the plasma axis is about 130 degree in the medium $\varepsilon_b$ configuration. In that case, the numerical calculation shows that CX-NPA observes passing particles. A clear dependence of the decay of the CX flux on bumpiness is found, i.e. the observed 1/e decay time of the CX flux after the NB turned-off, which is much smaller than the classical beam energy slowing down time as described below, increases with bumpiness.

From an aspect of the classical collision processes, the loss term of fast ion is mainly classified into orbit loss, pitch angle scattering, slowing-down, and charge exchange. The orbit calculation predicts that loss time of the ions where CX-NPA observes at $\phi_{NPA}$ = +12 $^o$ is longer than 5 ms and there is no difference on the bumpiness configuration, since these particles correspond passing particles. Figure 4 shows the time evolution of the loss rate of the energetic ions deduced by the orbit following calculation with the initial energy of 18 keV for the three bumpiness $\varepsilon_b$ cases [11]. The bumpiness dependence on the loss rate appears in the trapped particles, that is, growth of the loss rate becomes slower with bumpiness. This is consistent with the slow grad-$\boldsymbol{B}$ drift due to the control of bumpiness as expected. At the quasi-steady-state condition after t = 0.1 ms, the difference in the loss rate is 29 % and 25 % for the high- and low-$\varepsilon_b$ cases, respectively, which corresponds to the loss cone angle. The slowing-down time was estimated to be around 60 ms and its difference among

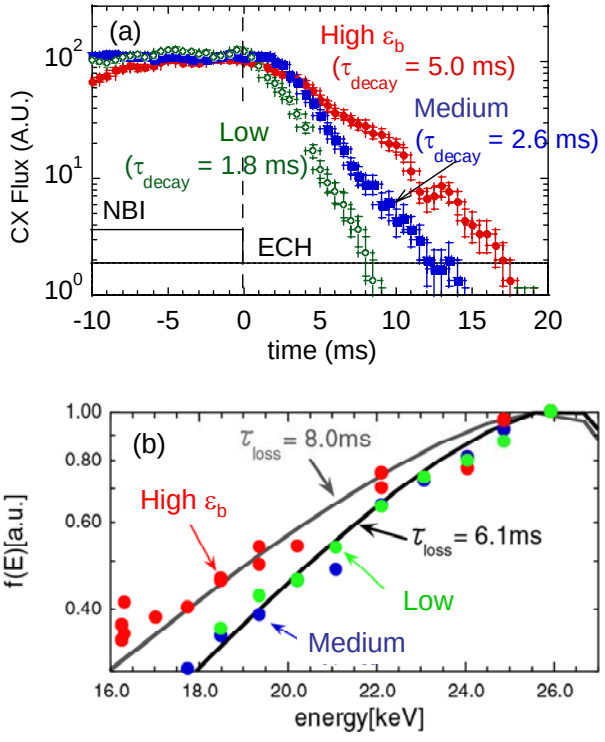


Fig. 3 (a) time evolution of the CX flux (E = 18 keV) just after the NB turned-off for high-, medium- and low-eb configurations, respectively, [11] and (b) energy spectrum obtained in the CX-NPA measurement and Fokker-Planck calculation. [12]

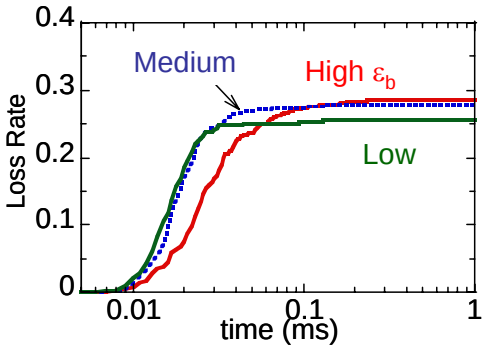


Fig. 4 Time evolution of the loss rate of fast ion ($E$ = 18 keV) deduced by the ion orbit following calculation for ion guiding center. The orbit calculation was done until the test particles from the initial position at $\rho$ = 0.25 strike the wall. [11]

the three configurations was negligibly small under the experimental condition. The CX loss time is considered to be unchanged in the experiments, since the $H_\alpha/D_\alpha$ intensity normalized by $\bar{n}_e$ did not change. In order to interpret the measurement result with CX-NPA, the Fokker-Planck analysis for the fast ion distribution is carried out using a zero-dimensional Fokker-Planck equation taking the effective loss time into account [12]. Figure 3(b) shows the measured and calculated CX energy spectra in the energy range from half- to full-energy of beam ion in the three bumpiness configurations. The effective loss time in the high-$\varepsilon_b$ configuration is longer than that for the medium and low-$\varepsilon_b$ cases. These results indicate that the effective confinement of the energetic ions improves as bumpiness increases.

### 3. 2. Energetic-ion-driven MHD activities

Interaction of fast ions with MHD activities is one of the most important issues in burning plasma physics, because it may decreases α-particle heating efficiency. In low-magnetic-shear helical devices, global Alfvén eighenmode (GAE) is a candidate of most unstable modes when fast ion pressure becomes fairly high. GAEs have been observed at several magnetic configurations in NBI plasmas of Heliotron J, however, strong bursting GAE has not been observed in low $\varepsilon_b$ configuration [13]. In order to investigate the ion transport in detail, we installed Hybrid Directional Langmuir probe (HDLP) system into Heliotron J [14]. HDLP can measure the co-directed and counter directed ion fluxes separately using some pairs of probe tip. This system can control the radial, poloidal and rotation angles simultaneously to detect the spatial distribution of fast ions and to align the pair of the probe tip with the magnetic field line.

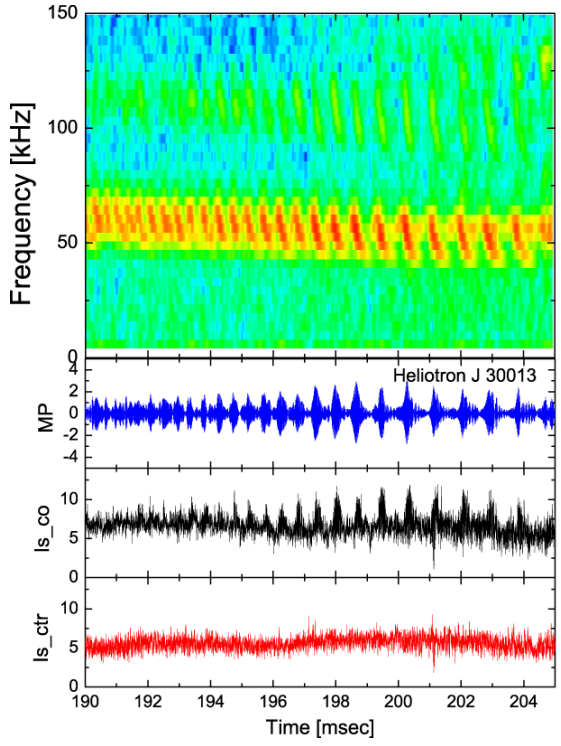


Fig. 5 The contour map of the power spectrum by magnetic fluctuation and its wave forms located on the chamber wall, co- and counter-directed (Is_co and Is_ctr) ion currents measured by HDLP at r/a= 0.9 [14].

Figure 5 shows the time evolution of the bursting GAE occurred in NBI and ECH plasmas [14]. The frequency of GAE chirped down quickly from 70 kHz to 40 kHz. The co-directed ion flux synchronized with GAE burst was observed and it was sensitive to the burst interval and amplitude. On the contrary, the response of the counter-going ion flux to GAE burst was weak. Then the co-going ion flux of fast ions is considered as a resonant convective oscillation [14]. These results indicate that the influence of GAE on the energetic ion confinement should be taken into account for further optimization of the helical-axis heliotron configuration toward fusion reactor.

### 4. Global Energy Confinement

In order to investigate the bumpiness effect on the energy confinement in NBI plasmas, we carried out bumpiness scan experiment in the NBI sustained plasmas. To clarify the absorbed power dependence, the power scan experiments are performed with keeping the line-averaged electron density almost constant. Figure 6 shows the plasma stored energy as a function of the absorbed NBI power ($P_{abs}$) in the three bumpiness configurations [15]. These data were obtained at the averaged electron density of $2\times10^{19}$ $m^{-3}$. The counter-direction neutral beam is injected to cancel out

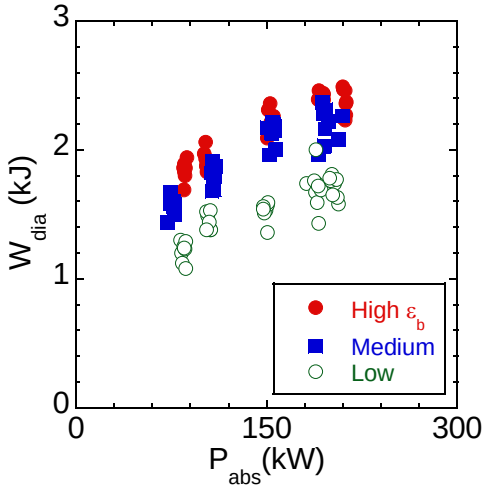


Fig. 6 Stored energy as a function of absorbed NBI power $P_{abs}$ obtained in high-, medium- and low-$\varepsilon_b$ configurations [15].

the change in the rotational transform by beta effects. The stored energy is evaluated by the diamagnetic loop data. The stored energy in the high- and medium-$\varepsilon_b$ configurations is clearly higher than that in the low $\varepsilon_b$ case. The difference of $W_{dia}$ between the high- and medium-$\varepsilon_b$ configurations is small, but the $W_{dia}$ in high-$\varepsilon_b$ case is more than 5% higher than that of the medium-$\varepsilon_b$ configuration.

The beam absorption profile and the total absorption rate are estimated by the following steps [16]; (1) calculation of birthpoints of the beam ions using Monte-Carlo method (HFREYA), (2) estimation of orbit loss and the redistribution of the beam ions by orbit calculation for ion guiding center (MCNBI) and (3) analysis of heating profile using Fokker-Planck equation (FIT) [17]. The Monte-Carlo code HFREYA is modified to apply the three-dimensional shape of the plasma and the inner vacuum vessel of Heliotron J. The ion orbit is calculated only at the initial energy of beam ions without slowing down process. The slowing down process of fast ions and the energy transfer to both the bulk electrons and ions are calculated by the Fokker-Planck analysis including the CX loss of fast ions. The density profiles are assumed to be parabolic. The shape of the radial profile of the electron (ion) temperature is also parabolic with the core temperature of 400 eV (300 eV). The edge neutral density is assumed to be $2\times10^{16}$ m$^{-3}$. In case of $\bar{n}_e$ = $2\times10^{19}$ m$^{-3}$, the absorption fractions is about 35 % for the three bumpiness configurations. The detailed evaluation of the orbit loss of fast ions including the slowing down process remains as a future work.

Figure 7(a) shows the bulk (deuterium) ion temperature deduced by CX-NPA as a function of the NBI absorption power $P_{abs}$ obtained in the three $\varepsilon_b$ configurations. A slightly increase in the ion temperature as increasing $\varepsilon_b$ is observed, that is, the ion temperature in the high, medium- and low-$\varepsilon_b$ configurations are 0.23, 0.20 and 0.18 keV at $P_{abs}$ of 200 kW, respectively. The ion temperature dependence on the NBI power is weak. As shown in Fig. 7(b), the electron cyclotron emission intensity ($I_{ECE}$) at the core region increased with $P_{abs}$ in high- and medium-$\varepsilon_b$ cases, while a relatively weaker dependence of the ECE intensity on $P_{abs}$ is obtained in the low-$\varepsilon_b$ configuration. The ECE measurement indicates an increase in the electron temperature both in high- and medium-$\varepsilon_b$ configurations. Although the calibrated ECE measurement is not available at present, the configuration dependence of the stored energy plotted in Fig. 6 can be explained qualitatively in terms of the difference in the electron temperature. The improvement in the electron temperature mainly contributes to the enhancement of the plasma performance in the two $\varepsilon_b$ configurations.

Figure 8 shows the comparison of the energy confinement time between experimentally obtained $\tau_E^{DIA}$ and International Stellarator Scaling law ISS95 $\tau_E^{ISS95}$ [18]. The energy confinement time is deduced by $\tau_E^{DIA} = (W_{dia} - W_{beam})/P_{abs}$, where $W_{beam}$ is the beam component of the stored energy deduced from the Fokker-Planck analysis, which is less than 7 % under these conditions. In the present experimental conditions, the electron

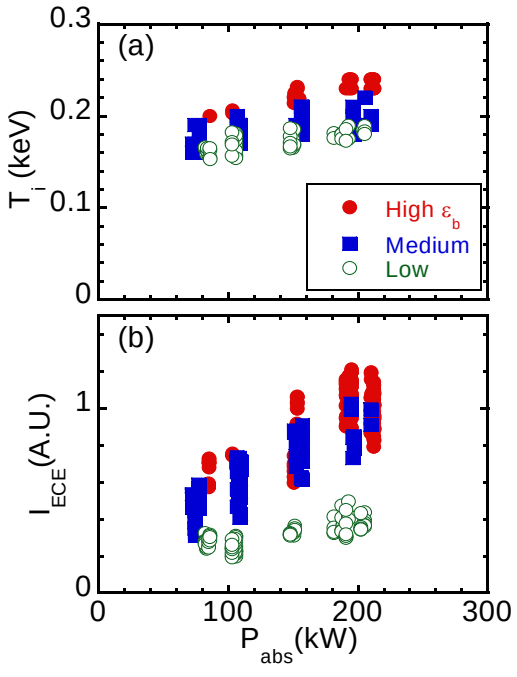


Fig. 7 (a) Bulk (deuterium) ion temperature and (b) ECE intensity as a function of $P_{abs}$ in high-, medium- and low-$\varepsilon_b$ configurations [15].

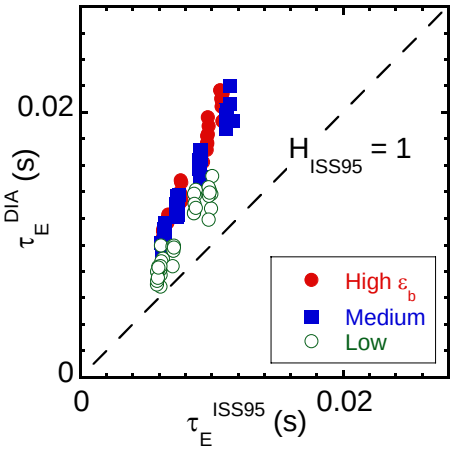


Fig. 8 Relationship between experimental energy confinement time and international empirical scaling law, ISS95, obtained in the NBI plasmas at the three bumpiness configurations [15].

collisionality is in the plateau regime. The enhancement factor of the energy confinement to the scaling ($H_{ISS95} = \tau_E^{DIA}/\tau_E^{ISS95}$) is about 1.8, 1.7 in the high and medium $\varepsilon_b$ configurations, respectively, which is higher than the low-$\varepsilon_b$ case of 1.4. These results suggest that the high and medium-$\varepsilon_b$ configurations have better confinement characteristics for bulk plasma than that for the low-$\varepsilon_b$ configuration in these experimental conditions.

Since the data shown in Fig. 8 were obtained at the constant density condition, the dependence of the energy confinement time on the heating power is investigated. Figure 9 shows the experimental energy confinement time as a function of NB absorption power. $\tau_E^{DIA}$ is proportional to $P_{abs}^{-0.72}$, $P_{abs}^{-0.66}$ and $P_{abs}^{-0.68}$ for the high-, medium- and low-$\varepsilon_b$ cases, respectively. The power dependence is almost similar to the ISS95 scaling ($\tau_E^{ISS95} \propto P^{-0.59}$), although the beam absorption was calculated under the assumed density and temperature profiles.

## 5. Summary

The energetic particle and global energy confinement in the NBI plasmas of Heliotron J has been investigated. The bumpiness control experiments have revealed the effectiveness of the control of bumpiness on the confinement both for the energetic particle and the bulk plasma. Under the present experimental conditions, the temperature dependence on bumpiness suggests that the electron energy transport mainly dominates the global energy confinement. Further experiments and analyses are needed to clarify the physical mechanism of the bumpiness effect on the anomalous electron transport.

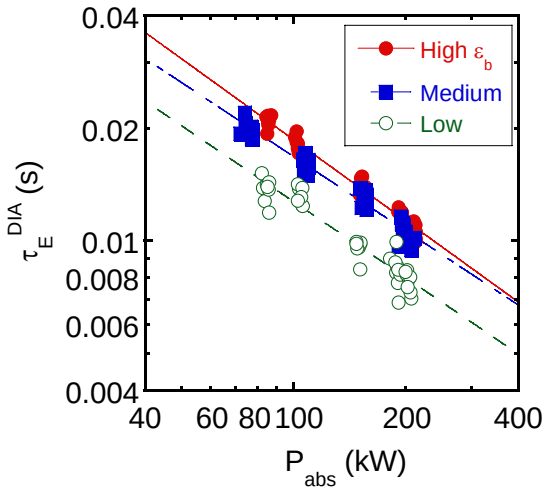


Fig. 9 Experimentally obtained energy confinement time as a function of NB absorption power.

## Acknowledgements

The authors thank the Heliotron J staff for conducting the experiments and discussions. This work was supported by NIFS/NINS under the NIFS Collaborative Research Program (NIFS04KUHL005, NIFS04KUHL003, NIFS04KUHL006, NIFS05KUHL007, NIFS06KUHL007, NIFS06KUHL010, NIFS07KUHL011, NIFS07KUHL015 and NIFS08KUHL020) and under a project sponsored by the Formation of International Network for Scientific Collaborations. This work was partly supported by a Grant-in-Aid for Scientific Research from the Japan Society for the Promotion of Science No. 20686061.

## References

[1] O. Motojima, et al., Nucl. Fusion **47** (2007) S668-S676.
[2] T. Obiki, et al., IAEA-CN-56/C-1-2 (1996).
[3] S. Okamura, et al., Nucl. Fusion **45** (2005) 863–870.
[4] S. Murakami, et al., Nucl. Fusion **42** (2002) L19–L22.
[5] H. Yamada, et al., Plasma Phys. Control. Fusion **43** (2001) A55–A71.
[6] S. Okamura, et Al 1999 Nucl. Fusion **39** (1999) 1337.
[7] F. Sano, et al., J. Plasma Fusion Res. SERIES **3** (2000) 26.
[8] T. Obiki, et al., Nucl. Fusion **41** (2001) 833.
[9] M. Wakatani, et al., Nucl. Fusion **40** (2000) 569.
[10] M. Yokoyama, et al., Nucl. Fusion **40** (2000) 261.
[11] S. Kobayashi, et al., IAEA-CN-116/EX/P4-41 (2004).
[12] M. Kaneko, et al., Fusion Sci. Tech. **50** (2006) 428.
[13] S. Yamamoto, et al., Fusion Sci. Tech. **51** (2007) 93.
[14] K. Nagaoka, et al., Proc. ICPP2008, P2-156 (2008).
[15] S. Kobayashi, et al., IAEA-CN-165/EX/P5-13 (2008).
[16] S. Murakami, et al., Trans. Fusion Tech. **27** (1995) 259.
[17] M. G. Mccoy, et al., Compt. Phys. Commu. **24** (1981) 37.
[18] U. Stroth, et al., Nuclear Fusion **36** (1995) 1063.